Received August 17, 2020, accepted August 23, 2020, date of publication August 31, 2020, date of current version September 14, 2020.

*Digital Object Identifier 10.1109/ACCESS.2020.3020270*

# S-Matrix and Bandpass Negative Group Delay Innovative Theory of Ti-Geometrical Shape Microstrip Structure

**XIANG ZHOU[1], (Member, IEEE), TAOCHEN GU[2], LILI WU[2], FAYU WAN[2], (Member, IEEE), BINHONG LI[3], NOUR MOHAMMAD MURAD[4], (Member, IEEE), SÉBASTIEN LALLÉCHÈRE[5], (Member, IEEE), AND BLAISE RAVELO[2], (Member, IEEE)**

[1]School of Mechanical Engineering, Southeast University, Nanjing 210096, China
[2]School of Electronic & Information Engineering, Nanjing University of Information Science and Technology, Nanjing 210044, China
[3]Key Laboratory of Silicon Device Technology, Chinese Academy of Sciences, Beijing 100029, China
[4]Energy Laboratory, Institut Universitaire de Technologie, 97410 Saint Pierre, France
[5]Université Clermont Auvergne, Institut Pascal, SIGMA Clermont, 63170 Aubiére, France

Corresponding author: Binhong Li (libinhong@ime.ac.cn)

This work was supported in part by the Opening Fund of Key Laboratory of Silicon Device and Technology, Chinese Academy of Sciences under Grant KLSDTJJ2019-04, and in part by the Postgraduate Research & Practice Innovation Program of Jiangsu Province under Grant KYCX20-0966.

**ABSTRACT** A theoretical investigation of distributed microwave circuit built with Ti-shape topology is developed. The topology under study consists of neighbored T- and i-shape interconnect lines. The Ti-topology equivalent S-matrix is calculated as a function of crosstalk coupling coefficient and coupled line (CL) delay. To highlight the NGD modelling feasibility, parametric analyses with respect to the T- and i-element coupling and delay are introduced. More practical validation is carried out with designed, simulated and measured microstrip prototype. It is found that because of T- and i-crosstalk, the Ti topology can behave as a bandpass NGD function. A good NGD performance with NGD level of approximately −1 ns around the center frequencies 2.2 GHz with transmission coefficient of approximately −2.1 dB and reflection coefficient better than −14 dB. The measured results are in good agreement with calculated models and simulations. Two-cell Ti-NGD circuits were also investigated to illustrate the designability of the topology for multi-band and widened single band NGD responses.

**INDEX TERMS** Crosstalk, distributed structure, Ti-topology, microwave theory, bandpass negative group delay (NGD), S-matrix theory.

## I. INTRODUCTION

To meet the requirements imposed by users' demands, the modern electronic devices must be designed with high performance printed circuit boards (PCBs). However, the design of high-performance PCB tends to be implemented with challenging technology based on integration density of high electrical interconnects and to operate with the high-speed signals.

Because of proximity between PCB interconnect lines and cables, undesirable effects as electromagnetic interference (EMI) and crosstalk coupling [1]–[4] are unavoidable and susceptible to degrade the electronic circuit performances. The crosstalk modelling becomes one of research topics attracting massively the electronic design, test and EMC research engineer attention [4]–[13]. Predictive approaches for analyzing PCB TL coupling need to be developed. Different computational and experimental methods for evaluating the crosstalk were proposed [5]–[12]. For example, probabilistic and statistical approaches [5], [9], [10] were developed for the crosstalk evaluation when the TL is relatively complex. But with the progress of TL configurations in the high-density PCB design, the statistical and also simulation-based tools [6] are not sometimes enough to provide understanding on specific phenomena behind the EMI and crosstalk coupling. Tentative approaches for eliminating TL crosstalk was suggested [13]. But further researches must go on to understand different effects associated to the EMI

The associate editor coordinating the review of this manuscript and approving it for publication was Andrei Muller.

and crosstalk coupling, especially, to facilitate the PCB SI and EMC analyses.

More specific modeling methodologies must be developed for predicting and understanding TL couplings. For example, it was found in [14]–[17], that the crosstalk between parallel coupled lines (CLs) can generate a particular phenomenon appearing with bandpass (BP) negative group delay (NGD). Basic study with coupling matrix approaches were conducted for analyzing the BP NGD effect [15], [16]. This particular phenomenon which is actually not familiar to the EMC research communities was singularly found with signal interference [17].

However, the NGD generation with significant NGD figure-of-merit (FoM) is accompanied by excessive insertion loss more than 20 dB [18], [19]. To challenge to reduce the attenuation lower than 10 dB. The design feasibility of NGD distributed microwave circuit which may not need lumped circuits was confirmed [17], [20]. Further challenge on the compact NGD circuit design was also made in [21]–[23]. In term of implementation, one of the most performing distributed NGD circuit designs are based on the use of transmission line (TL) and coupled lines (CLs) [20], [24], [25]. Some of TL NGD networks can be typically accomplished by using TL stubs with loaded resistors. By using a distributed TL, a novel design method of the filter based on the NGD circuit is reported [26] and the GD can be perfectly controlled by the resistors. Because of L and C lumped element design limitations, most of NGD topologies cannot be integrated in high speed systems. To target lower signal attenuation with fully distributed circuit, two short-circuited CLs with high characteristic impedance and small coupling coefficient were designed. This CL-based NGD circuit is able to decrease the attenuation to 7.43 dB [27]. An NGD topology built with parallel interconnect line was theorized and designed. This parallel interconnect line NGD circuit is able to operate with attenuation of about 4 dB [17]. More recently, further design effort and conducted to design an NGD circuit consists of interconnect line coupled with a radial stub terminated line which presents 3.1 dB insertion loss [28]. It is still necessary to realize further research works must be done about NGD circuit topologies with new design variety, analytical modelling method notably with low attenuation.

For this reason, in this paper, an innovative NGD theory of TL passive topology with consideration of EMI crosstalk and further challenge on CL delay effect is developed. The topology under investigation is constituted by a particular ''Ti''-shape geometry. This particularly simple structure is built with an open-ended CL and an access TL.

The paper is mainly organized in five different sections described as follows:

- The Ti topology will be introduced and described in Section II. The analytical equivalent S-matrices of each constituting elements of the Ti structure will be also presented.
- The S-matrix model will be established in Section III. Then, the frequency responses including the group delay (GD) will be analyzed with respect to the Ti topology parameters.
- The experimental investigation on the unfamiliar phenomenon induced in the Ti microstrip proof-of-concept (POC) is validated in Section IV. Excellent comparisons between calculation, simulation and measurement will be discussed.
- Section V is focused on the feasibility study of dual-band and widened NGD band circuits with the Ti-topology.
- Then, the conclusion of the paper is presented in Section VI.

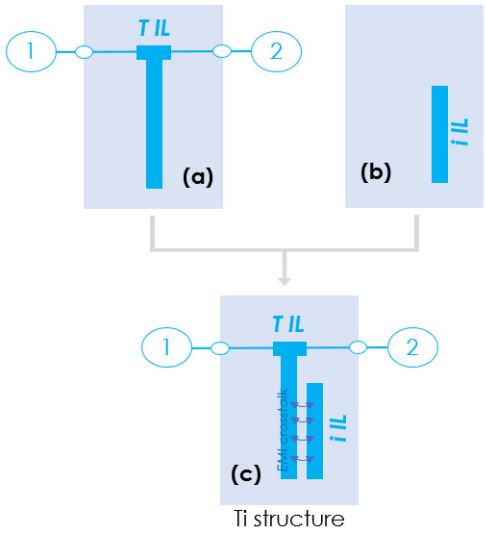


**FIGURE 1.** Configuration of (a) "T", (b) "i" and (c) "Ti" two-port structures.

## II. DESCRIPTION OF THE CROSSTALK Ti STRUCTURE AND CONSTITUTING ELEMENT S-MATRICES

The present section investigates the analytical approach on the ''Ti'' TL structure. After the topological analysis, the equivalent circuit diagram is introduced. The S-parameter modeling is developed by considering the ''T'' and ''i'' element of the constituting elementary block components.

### A. DESCRIPTION OF THE Ti GEOMETRICAL SHAPE STRUCTURE

Fig. 1(a), Fig. 1(b) and Fig. 1(c) introduce the configurations of the ''T'', ''i'' and ''Ti'' TL structures under study, respectively. This innovative NGD topology is implemented as a two-port circuit referenced by Port ① and Port ②.

Under the considered configuration, this Ti-shape circuit can be assumed as a scenario of a victim ''T'' TL by the crosstalk perturbation due to the ''i'' TL. The T TL behaves as an open ended $TL_T(R_0, \alpha, \tau)$ by the characteristic impedance $R_0 = 50\Omega$, attenuation, $a$, and delay, $\tau$. The ''i'' TL is also supposed ideally with the same characteristics. Before the EMI crosstalk study onto the Ti TL, the single T structure S-matrix will be introduced in the next subsection.

### B. S-MATRIX MODEL OF OPEN-ENDED STUB STRUCTURE

As an elementary block of the "Ti" structure, it would be important to start with the S-matrix model of "T" corresponding open-ended stub structure.

#### 1) LOSSY TL S-MATRIX

We assume that the TL constituting the Ti topology as an ideally matched line integrating the attenuation loss and propagation delay. Therefore, the TL can be represented as $TL_T(R_0, \alpha, \tau)$. For the analytical representation, such a TL can be modelled with the S-matrix:

$$[S(s)] = \begin{bmatrix} 0 & \alpha\, x(s) \\ \alpha\, x(s) & 0 \end{bmatrix}. \tag{1}$$

with $s$ represents the Laplace variable, the delay propagator can be expressed as:

$$x(s) = e^{-s\tau}. \tag{2}$$

#### 2) Li-TOPOLOGY S-MATRIX MODEL

The S-matrix of two-port circuit corresponding T-shape TL of Fig. 1(a) can be written as:

$$\left[S^T(s)\right] = \begin{bmatrix} S_{11}^T(s) & S_{12}^T(s) \\ S_{21}^T(s) & S_{22}^T(s) \end{bmatrix}. \tag{3}$$

Acting as a symmetrical passive circuit, the reflection and transmission coefficients must satisfy the relations:

$$S_{11}^T(s) = S_{22}^T(s) \tag{4}$$
$$S_{21}^T(s) = S_{12}^T(s). \tag{5}$$

Based on the TL theory, the reflection and transmission coefficients can be written as follows, respectively:

$$S_{11}^T(s) = \frac{1 - \alpha^2 x^2(s)}{3 + \alpha^2 x^2(s)} \tag{6}$$
$$S_{21}^T(s) = \frac{2\left[1 + \alpha^2 x^2(s)\right]}{3 + \alpha^2 x^2(s)}. \tag{7}$$

### C. DEDUCTION OF S-MATRIX GLOBAL MODEL OF THE Ti TOPOLOGY

Before the analytical theory, it is worth to describe the equivalent topology of the Ti structure under study.

#### 1) TOPOLOGICAL ALGEBRAIC INVESTIGATION OF THE Ti STRUCTURE

The electrical diagram equivalent to the Ti circuit can be represented as introduced in Fig. 2. This diagram can be assumed as composed of the following elementary blocks:

i) A short-circuited Tee power divider (PWD) which is three-port system with terminal ports numbered ①, ② and ③,
ii) And a four-port CL including the crosstalk between T and i with terminal ports numbered ③, ④, ⑤ and ⑥.

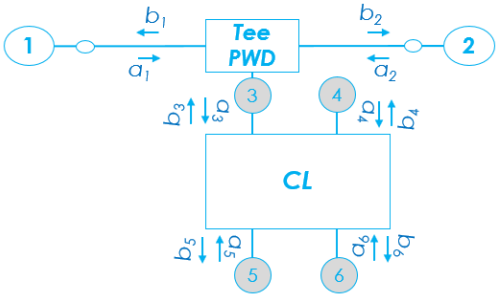


**FIGURE 2.** Equivalent topological diagram of the Ti structure introduced in Fig. 1(c).

#### 2) S-MATRIX MODEL OF TEE POWER DIVIDER

According to S-parameter theory, the ideal Tee PWD equivalent S-matrix is given by:

$$\left[S^{PWD}\right] = \begin{bmatrix} -1/3 & 2/3 & 2/3 \\ 2/3 & -1/3 & 2/3 \\ 2/3 & 2/3 & -1/3 \end{bmatrix}. \tag{8}$$

Hence, the relationship between the input/output wave powers $a_m$ and $b_m (m = \{1, 2, 3\})$ passing through the Tee ports can be explained by the following basic equation:

$$\begin{bmatrix} b_1(s) \\ b_2(s) \\ a_3(s) \end{bmatrix} = \left[S^{PWD}\right] \times \begin{bmatrix} a_1(s) \\ a_2(s) \\ b_3(s) \end{bmatrix}. \tag{9}$$

#### 3) S-MATRIX OF CL ELEMENT CONSITUTING THE Ti TOPOLOGY

The CL of Fig. 2 is assumed as a four-port network with port numbers ③,④,⑤ and ⑥. By taking the EMI crosstalk coupling coefficient, $\zeta$, between the two constituting parallel TL, we denote:

$$\varsigma(s) = \zeta\, e^{-s\tau/2}. \tag{10}$$

With this parameter, the S-matrix model of the CL block can be written as:

$$\left[S^{CL}(s)\right] = \begin{bmatrix} 0 & \varsigma(s) & \xi(s) & 0 \\ \varsigma(s) & 0 & 0 & \xi(s) \\ \xi(s) & 0 & 0 & \varsigma(s) \\ 0 & \xi(s) & \varsigma(s) & 0 \end{bmatrix}. \tag{11}$$

We emphasize that in addition to the originality of the Ti topology analysis, the current work does not need extra lossy resistor as in [29], [30], and the Ti NGD structure is small comparatively to the works given in [31]. Moreover, we would like to point out that in difference to the CL based NGD investigated in [15], [28], the present S-matrix modelling is developed with consideration of the CL attenuation and delay denoted $\alpha < 1$ and $\tau$, respectively. The S parameter of the CL $[S_{CL}]$ $\xi$ is expressed as:

$$\xi(s) = -\alpha\, e^{-s\tau}\varpi \tag{12}$$

and

$$\varpi = \sqrt{1 - \zeta^2}. \tag{13}$$

Following the configuration of CL with four ports displayed in Fig. 1(b), this four-dimension S-matrix related to the wave ports $a_m$ and $b_m$ ($m = \{3, 4, 5, 6\}$) can be expressed by the relations:

$$\begin{bmatrix} a_3(s) \\ a_4(s) \\ a_5(s) \\ a_6(s) \end{bmatrix} = \left[S^{CL}(s)\right] \times \begin{bmatrix} b_3(s) \\ b_4(s) \\ b_5(s) \\ b_6(s) \end{bmatrix}. \tag{14}$$

## III. THEORIZATION OF THE Ti-TOPOLOGY FOR BP NGD ANALYSIS

Based on the previous constituting element S-matrices, the Ti equivalent model will be established. Then, the group delay (GD) phenomenological analysis will be developed in the present section. The Ti topology NGD analysis will be performed around its operating frequency.

### A. S-MATRIX CALCULATION MECHANISM OF Ti TOPOLOGY

The present subsection develops the calculation mechanism of the S-matrix of the Ti topology.

#### 1) S-MATRIX REPRESENTATION

Knowing that the Ti topology under investigation is a two-port system, the equivalent S-matrix can be expressed as:

$$\left[S^{Ti}(s)\right] = \begin{bmatrix} S_{11}^{Ti}(s) & S_{12}^{Ti}(s) \\ S_{21}^{Ti}(s) & S_{22}^{Ti}(s) \end{bmatrix}. \tag{15}$$

Similar to the previous symmetric passive T structure, the input and output reflection coefficients, and the forward and backward transmission coefficients are identical:

$$\begin{cases} S_{11}^{Ti}(s) = S_{22}^{Ti}(s) \\ S_{12}^{Ti}(s) = S_{21}^{Ti}(s). \end{cases} \tag{16}$$

#### 2) S-MATRIX ALGEBRAIC CALCULATION

The algebraic calculation of previously represented 2-D S-matrix is based on the algebraic operation between the input and output wave powers interacting between the elementary blocks of Fig. 2. Substantially, the analytical expression of this S-matrix is determined from substitution of wave powers in matrix relationships (9) and (14) to get the global matrix equation:

$$\begin{bmatrix} b_1(s) \\ b_2(s) \end{bmatrix} = \left[S^{Ti}(s)\right] \times \begin{bmatrix} a_1(s) \\ a_2(s) \end{bmatrix} \tag{17}$$

By identification, the Ti topology S-matrix elements which are the coefficients of input power waves $a_1$ and $a_2$ are expressed as:

$$S_{11}^{Ti}(s) = \frac{\begin{array}{l} -\alpha^4\varpi^4x^4(s) + 2\alpha^2\zeta^2\varpi^2x^3(s) \\ +(2\alpha^2\varpi^2 - \zeta^4)x^2(s) + 2\zeta^2x(s) - 2 \end{array}}{D(s)} \tag{18}$$

$$S_{21}^{Ti}(s) = \frac{2\left[\alpha^4\varpi^4x^4(s) - 2\alpha^2\zeta^2\varpi^2x^3(s) + \zeta^2x^2(s) - 1\right]}{D(s)} \tag{19}$$

with:

$$D(s) = \begin{bmatrix} \alpha^4\varpi^4x^4(s) - 2\alpha^2\varpi^2\zeta^2x^3(s) \\ +(2\alpha^2\varpi^2 + \zeta^4)x^2(s) + 2\zeta^2x(s) - 3 \end{bmatrix}. \tag{20}$$

#### 3) SRECALL ON THE FREQUENCY-DEPENDENT S-PARAMETERS AND GD

In the following part of the section, we assume that the angular frequency variable $\omega$ by taking $s = j\omega$. To perform the frequency domain analysis, we will use the reflection and transmission coefficient magnitudes:

$$S_{11}^{Ti}(\omega) = \left|S_{11}^{Ti}(j\omega)\right| \tag{21}$$

$$S_{21}^{Ti}(\omega) = \left|S_{21}^{Ti}(j\omega)\right|. \tag{22}$$

Then, particular attention will be paid on the transmission phase:

$$\varphi(\omega) = \angle S_{21}^{Ti}(j\omega). \tag{23}$$

This quantity will serve for the elaboration of the Ti topology GD. By definition, the GD is written as:

$$GD(\omega) = -\frac{\partial\varphi(\omega)}{\partial\omega}. \tag{24}$$

The next subsection will explore these S-parameters and GD to perform the phenomenological analyses of the Ti topology crosstalk effect.

### B. MAGNITUDE AND PHASE EXPRESSIONS OF S-PARAMETERS

Based on the previously introduced S-matrix, the reflection and transmission coefficients are expressed in the following paragraph.

#### 1) MAGNITUDE EXPRESSIONS

The magnitudes of the reflection and transmission coefficients defined in (18) and (19), respectively can be expressed as:

$$S_{11}^{Ti}(\omega) = \sqrt{\frac{Rn_{11}^2(\omega) + In_{11}^2(\omega)}{Rd_{11}^2(\omega) + Id_{11}^2(\omega)}} \tag{25}$$

$$S_{21}^{Ti}(\omega) = \sqrt{\frac{Rn_{21}^2(\omega) + In_{21}^2(\omega)}{Rd_{21}^2(\omega) + Id_{21}^2(\omega)}} \tag{26}$$

where:

$$Rn_{11}(\omega) = 2\begin{bmatrix} 2\alpha^2\zeta^2(1-\zeta^2)\cos(\tau\omega) \\ +\left[2\alpha^2(1-\zeta^2) - \zeta^4\right]\cos(2\tau\omega) \\ +2\zeta^2\cos(3\tau\omega) - \cos(4\tau\omega) \\ -\alpha^4(\zeta^2-1)^2 \end{bmatrix} \tag{27}$$

$$In_{11}(\omega) = 2\begin{bmatrix} 2\alpha^2\zeta^2(\zeta^2-1)\sin(\tau\omega) \\ +\zeta^4\sin(2\tau\omega) - \sin(4\tau\omega) \end{bmatrix} \tag{28}$$

$$Rn_{21}(\omega) = 2\begin{bmatrix} 2(\zeta^4+4)\cos^2(\tau\omega) - 8\cos^4(\tau\omega) \\ +2\alpha^2\zeta^2(\zeta^2-1)\cos(\tau\omega) \\ +\alpha^4(1-\zeta^2)^2 - 1 - \zeta^4 \end{bmatrix} \tag{29}$$

$$In_{21}(\omega) = 2\begin{bmatrix} 2\alpha^2\zeta^2(\alpha^2\zeta^2-1)\sin(\tau\omega) \\ +\zeta^2\sin(2\tau\omega) - \sin(4\tau\omega) \end{bmatrix} \tag{30}$$

$$Rd_{11}(\omega) = Rd_{21}(\omega) = \left\{ \begin{array}{l} \alpha^4(1-\zeta^2)^2 \\ +2\alpha^2\zeta^2(\zeta^2-1)\cos(\tau\omega) \\ +\left[\zeta^4+2\alpha^2(1-\zeta^2)\right]\cos(2\tau\omega) \\ +2\zeta^2\cos(3\tau\omega)-3\cos(4\tau\omega) \end{array} \right\} \tag{31}$$

$$Id_{11}(\omega) = Id_{21}(\omega) = \left\{ \begin{array}{l} 2\alpha^2\zeta^2(\zeta^2-1)\sin(\tau\omega) \\ +\left[\zeta^4+2\alpha^2(1-\zeta^2)\right]\sin(2\tau\omega) \\ \\ +2\zeta^2\sin(3\tau\omega)-3\sin(4\tau\omega) \end{array} \right\}. \tag{32}$$

#### 2) EXPRESSION OF TRANSMISSION PHASE

The Ti topology transmission phase defined in (23) is given by:

$$\varphi(\omega) = \varphi_n(\omega) - \varphi_m(\omega) \tag{33}$$

where:

$$\varphi_n(\omega) = \arctan\left[\frac{\begin{array}{l} 2\alpha^2\zeta^2(\alpha^2\zeta^2-1)\sin(\tau\omega) \\ +\zeta^2\sin(2\tau\omega)-\sin(4\tau\omega) \end{array}}{\begin{array}{l} 2(\zeta^4+4)\cos^2(\tau\omega)-8\cos^4(\tau\omega) \\ +2a^2\zeta^2(\zeta^2-1)\cos(\tau\omega) \\ +\alpha^4(1-\zeta^2)^2-1-\zeta^4 \end{array}}\right] \tag{34}$$

$$\varphi_m(\omega) = \arctan\left[\frac{\begin{array}{l} 2\alpha^2\zeta^2(\zeta^2-1)\sin(\tau\omega) \\ +\left[\zeta^4+2\alpha^2(1-\zeta^2)\right]\sin(2\tau\omega) \\ +2\zeta^2\sin(3\tau\omega)-3\sin(4\tau\omega) \end{array}}{\begin{array}{l} \alpha^4(1-\zeta^2)^2+2\alpha^2\zeta^2(\zeta^2-1)\cos(\tau\omega) \\ +\left[\zeta^4+2a^2(1-\zeta^2)\right]\cos(2\tau\omega) \\ +2\zeta^2\cos(3\tau\omega)-3\cos(4\tau\omega) \end{array}}\right]. \tag{35}$$

### C. NGD ANALYSIS OF THE Ti TOPOLOGY

The NGD analysis of the Ti topology will be explored in the following paragraph.

#### 1) GD DEFINITION

To do this, the GD was transitively derived from definition (24) by means of transmission phase expressed in (33). Subsequently, the Ti topology GD can be calculated with the equation:

$$GD(\omega) = \frac{\partial\left[\varphi_m(\omega)-\varphi_n(\omega)\right]}{\partial\omega}. \tag{36}$$

#### 2) NGD CENTER FREQUENCY

The behavioral NGD approach allows to state that the NGD center frequency, $f_0$, related to:

$$\omega_0 = 2\pi f_0 \tag{37}$$

corresponds to the frequency where the GD may achieve its optimal value. As the study is focused on the negative part of the GD, this optimal value can be equal to the minimal one:

$$GD_0 = GD(\omega_0) = \min\left[GD(\omega)\right]. \tag{38}$$

For the Ti topology under study, this center frequency corresponds to the loaded CL resonance frequency which can be written in function of the CL delay:

$$f_0 = \frac{1}{2\tau_c}. \tag{39}$$

#### 3) S-PARAMETER MAGNITUDES AT NGD CENTER FREQUENCIES

At the center frequency,

$$\omega = \omega_0 \tag{40}$$

the associated reflection and transmission coefficient magnitudes previously introduced in (25) and (26), respectively, can transformed as:

$$S_{11}(\omega_0) = \left|\frac{2\alpha^2(\alpha^2-2)\zeta^2-(1-\alpha^2)^2(\zeta^4+1)}{\begin{array}{l}(1-\alpha^2)^2\zeta^4-2(1+\alpha^4)\zeta^2 \\ +(\alpha^2-1)(\alpha^2+3)\end{array}}\right| \tag{41}$$

$$S_{21}(\omega_0) = \frac{2(1-\zeta^2)(1-\alpha^2)\left[(1-\alpha^2)\zeta^2+1+\alpha^2\right]}{\left|\begin{array}{l}(1-\alpha^2)^2\zeta^4-2(1+\alpha^4)\zeta^2 \\ +(\alpha^2-1)(\alpha^2+3)\end{array}\right|}. \tag{42}$$

#### 4) GD EXPRESSION AT NGD CENTER FREQUENCIES

The GD response was obtained after mathematical calculation of the expression given in (28). After simplification at the center frequency, this GD becomes:

$$\tau_{Ti}(\omega_0) = \frac{2\tau(N_0+N_2\zeta^2+N_4\zeta^4+N_6\zeta^6)}{(1-\alpha^2)(1-\zeta^2)(D_0+D_2\zeta^2+D_4\zeta^4)} \tag{43}$$

with:

$$\left\{ \begin{array}{l} N_6 = (1-\alpha^2)(2\alpha^4+3\alpha^2-1) \\ N_4 = 2(3\alpha^6-\alpha^4+\alpha^2-1) \\ N_2 = -6\alpha^6+7\alpha^4-8\alpha^2-1 \\ N_0 = 2\alpha^2(\alpha^2-1)^2 \end{array} \right. \tag{44}$$

$$\left\{ \begin{array}{l} D_4 = (\alpha^2-1)^2 \\ D_2 = -2(\alpha^4+1) \\ D_0 = \alpha^4+2\alpha^2-3. \end{array} \right. \tag{45}$$

### D. DESIGN FLOW OF THE Ti NGD CIRCUIT

The design method of Ti topology-based BP NGD passive circuit is practically analog to the classical RF and microwave microstrip circuits. For the RF and microwave non-specialist engineers, the design flow of this BP NGD passive circuit can be organized in the following seven successive actions:

Action 1: The design process must begin with the desired BP NGD specifications as the NGD center frequency, NGD value, insertion loss and reflection loss.

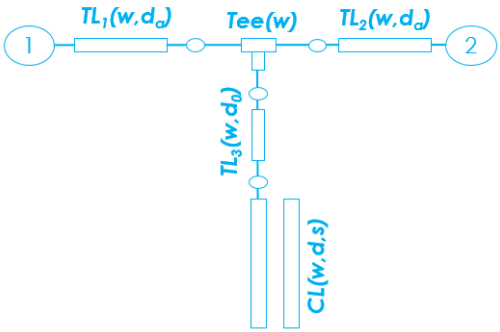


**FIGURE 3.** Design parameters of Ti prototype.

Action 2: Schematic circuit simulations in the expected operation frequency range.
Action 3: According to the fabrication constraints, the minimal and maximal ranges of the physical parameters must be defined.
Action 4: After the 2-D or 3-D design of the passive circuit (in the present study limited to microstrip technology), the physical sizes of the widths, lengths and interspaces constituting the structure should be optimized.
Action 5: The fabrication of the BP NGD circuit final design should be realized after probable otimization.
Action 6: Then, the final stage will be BP NGD béhavioral validation tests of the prototype.

The practical phenomenological analysis behind the crosstalk effect on the Ti topology will be investigated in the next section.

## IV. SIMULATED AND MEASURED BP NGD VALIDATION RESULTS OF Ti NGD POC

The current section is mainly devoted to the verification of the previously established S-parameter theory of the Ti topology. As a POC, a microstrip Ti circuit was designed and simulated by using microwave circuit software ADS® from Keysight Technologies® . Sensitivity analyses will be introduced with respect to crosstalk parameters. Then, simulation and measurement results will be presented for the experimental validation.

### A. DESCRIPTION OF Ti NGD POC

Fig. 3 represents the POC of the Ti topology circuit design from the ADS® schematic environment. For the comfortability of the measurement configuration, extra access lines $TL_1$, $TL_2$ and $TL_3$ were added in the circuit. In this design, the Ti circuit is composed of:

- two-port access lines named $TL_1$ and $TL_2$, defined physical width, $w$, and length, $d_a$,
- Tee connector with physical width $w$,
- $TL_3$ defined physical width, $w$, and length, $d_0$,
- and a CL physical width, $w$, and length, $d_a$, and space, $s$.

The 3-D design view and the photograph of the fabricated circuit are shown in Fig. 4(a) and in Fig. 4(b)

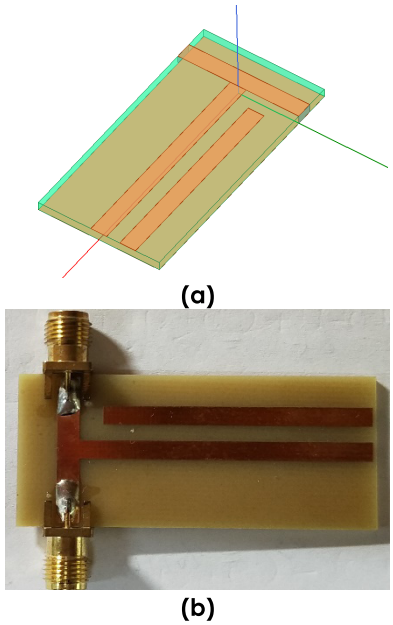


**FIGURE 4.** (a) 3D HFSS® design and (b) photograph of Ti POCs.

respectively. The tested Ti prototype presents the physical size, 24 mm × 46 mm. The Ti topology POC was implemented on Cu metallized FR4-epoxy substrate presenting related parameters addressed in Table 1. Moreover, the fabricated Ti circuit geometrical parameters are also summarized in this Table 1.

**TABLE 1.** Physical and geometrical parameters of the Ti prototype shown in Figs. 4.

| *Constituting element* | *Designation* | *Parameters* | *Values* |
|---|---|---|---|
| Substrate | Dielectric substrate | $h$ | 1.6 mm |
| | thickness | | |
| | Relative permittivity | $\varepsilon_r$ | 5.1 |
| | Metallization thickness | $t$ | 35 µm |
| | Loss tangent | $\tan(\delta)$ | 0.02 |
| | Metallization conductivity | $\sigma$ | 58 MS/m |
| CL | Width | $w$ | 3 mm |
| | Length | $d$ | 35 mm |
| | Interspace | $s$ | 2.5 mm |
| Access lines $TL_1/TL_2$ | Length | $d_a$ | 5 mm |
| | Width | $w$ | 3 mm |
| Access lines $TL_1/TL_2$ | Length | $d_1$ | 5 mm |
| | Width | $w$ | 3 mm |

### B. PARAMETRIC ANALYSES WITH RESPECT TO THE CL CHARACTERISTICS

The implemented parametric analyses aim to predict the influences of the Ti topology parameters, $w$, $d$ and $s$ on the NGD function. Three cases of S-parameter parametric simulations from ADS® were performed by changing $d$, $w$ and $s$. The obtained simulated results about GD, $S_{21}$ and $S_{11}$ are keenly mapped in cartography in function of the concerned physical variable and the frequency.

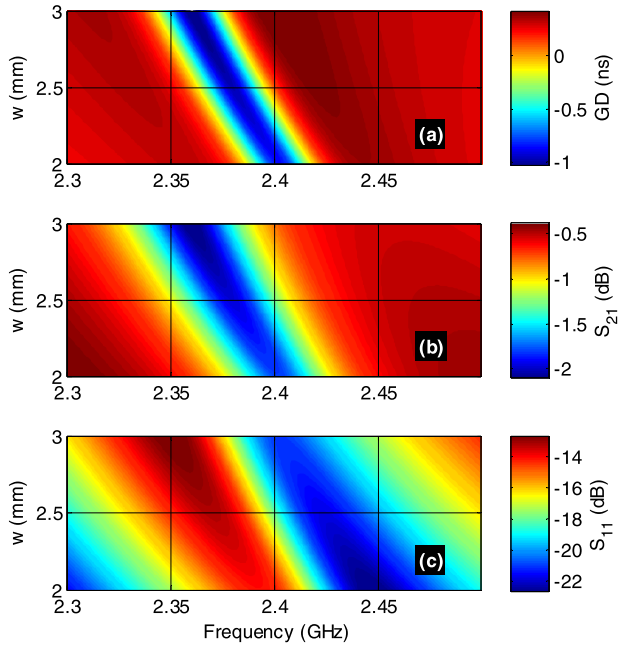


**FIGURE 5.** Parametric analysis results versus w: (a) GD, (b) $S_{21}$ and (c) $S_{11}$.

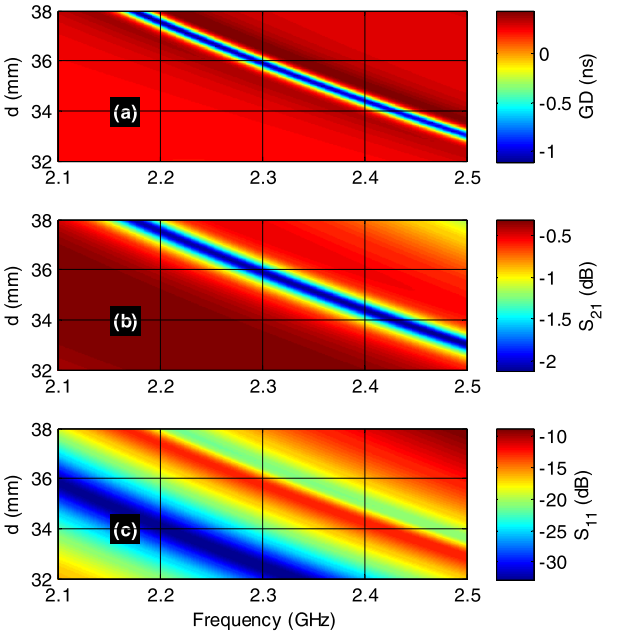


**FIGURE 6.** Parametric analysis results versus d: (a) GD, (b) $S_{21}$ and (c) $S_{11}$.

**TABLE 2.** NGD specifications versus CL width, *w*.

| *w*(mm) | *Z*(Ω) | $f_0$(GHz) | $GD(f_0)$(ns) | $S_{21}(f_0)$(dB) | $S_{11}(f_0)$(dB) |
|---|---|---|---|---|---|
| 2 | 63 | 2.249 | -1.329 | -2.431 | -12.484 |
| 2.5 | 55.9 | 2.226 | -1.274 | -2.309 | -12.700 |
| 3 | 50.3 | 2.206 | -1.196 | -2.257 | -11.480 |

**TABLE 3.** NGD specifications versus CL length, *d*.

| *d* (mm) | *Electrical length* | $f_0$ (GHz) | $GD(f_0)$ (ns) | $S_{21}(f_0)$ (dB) | $S_{11}(f_0)$ (dB) |
|---|---|---|---|---|---|
| 32 | 180° | 2.411 | -1.086 | -2.282 | -11.415 |
| 35 | 180° | 2.206 | -1.196 | -2.257 | -11.480 |
| 38 | 183° | 2.032 | -1.308 | -2.238 | -11.556 |

### 1) PARAMETRIC ANALYSIS WITH RESPECT TO THE CL PHYSICAL WIDTH

This present section introduces the influence of the CL width $w$. During the simulations, this later one is varied from 2 mm to 3 mm with fixed $s = 2.5$ mm and $d = 35$ mm. The parametric S-parameters were considered from 2.3 to 2.55 GHz. The cartographies of the GD, $S_{21}$ and $S_{11}$ simulated results are displayed in Figs. 5(a), 5(b) and 5(c), respectively. It can be found from Fig. 5(a) that the Ti POC behaves as a BP NGD function. The NGD center frequency varies inversely to $w$. More specifically, the center frequency of the circuit shifts to the left by about 20 MHz when the CL width increases. However, the NGD absolute value is less sensitive to the CL width. Fig. 5(b) illustrates that the change of insertion loss $S_{21}$. This later one has a similar trend to GD. It is important to emphasize here that $S_{21}$ presents very low attenuation less than 2.5 dB. As can be seen from Fig. 5(c), reflection loss $S_{11}$ is better than 10 dB in the considered range of the CL width and the frequency band. Table 2 summarizes the simulation results.

### 2) PARAMETRIC ANALYSIS WITH RESPECT TO THE CL LENGTH

Figs. 6 indicate the variation of the Ti circuit GD and S-parameter when the CL length $d$. During the simulations, this later one was varied from 32 mm to 38 mm. Then, the CL width $w$ and space $s$ are kept equal to 3 mm and 2.5 mm, respectively. Fig. 6(a) shows that the BP NGD response with the NGD center frequency can be controlled by the CL length. When $d$ gradually increases, the NGD center frequency is shifting from approximately 2.17 GHz to 2.5 GHz and the GD changes from $-1.082$ ns to $-1.308$ ns. In addition, as illustrated in Fig. 6(b) and Fig. 6(c), $S_{21}$ and $S_{11}$ are kept basically unchanged. Therefore, we can change the length of the coupled line to adjust the specified NGD center frequency. Table 3 summarizes the parametric simulation respect to CL length, $d$, varies from 32 mm to 38 mm.

### 3) PARAMETRIC ANALYSIS WITH RESPECT TO THE CL PHYSICAL INTERSPACE

The present paragraph analyses the influence of the coupling space $s$ by fixing $w = 3$ mm and $d = 35$ mm on the Ti POC NGD performance. The S-parameters and GD in function coupling space $s$ are addressed in Figs. 7. From these simulated results, it can be underlined that the GD and $S_{21}$ decrease when $s$ varies from 2 to 3 mm. However, reflection loss $S_{11}$ becomes better with the increase of $s$. Larger absolute value of $s$ implies small GD absolute value, low attenuation loss and good reflection coefficient. Table 4 summarizes the

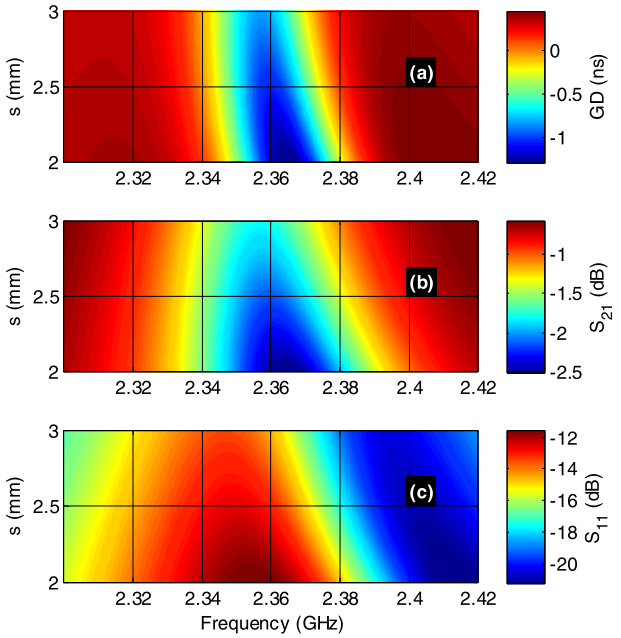


**FIGURE 7.** Parametric analysis results versus s: (a) GD, (b) $S_{21}$ and (c) $S_{11}$.

**TABLE 4.** NGD specifications versus CL space, *s*.

| *s* (mm) | *K* (dB) | $f_0$ (GHz) | $GD(f_0)$ (ns) | $S_{11}(f_0)$ (dB) | $S_{21}(f_0)$ (dB) |
|---|---|---|---|---|---|
| 2 | -19.5 | 2.211 | -1.498 | -2.703 | -10.511 |
| 2.5 | 21.4 | 2.206 | -1.196 | -2.257 | -11.480 |
| 3 | 23.2 | 2.203 | -0.936 | -1.893 | -12.359 |

parametric simulation respect to CL interspace, *s*, varies from 2 mm to 3 mm.

### C. EXPERIMENTAL INVESTIGATION

To validate more concretely the Ti topology theory established in Section III, experimental investigation was conducted. Comparisons between the calculated results from the analytical model and simulations confirmed with measurements will be examined in the following subsections.

#### 1) EXPERIMENTAL SETUP

The fabricated NGD circuit was measured with a VNA provided by Rohde & Schwarz (ZNB 20, frequency band 100 kHz to 20 GHz). The S-parameter measurement experimental setup with the POC Ti circuit is shown in Fig. 8.

The experimental measurements were spanned in the frequency domain from 2 GHz to 2.5 GHz.

#### 2) DISCUSSION ON MODELED, SIMULATED AND MEASURED RESULTS

Comparisons between a single T simulated response and Ti calculated, simulated and measured S-parameters and GDs were displayed in Figs. 9. Due to the T and i element crosstalk, obvious differences between the single T and Ti S-parameters is observed. This result reveals obviously that the

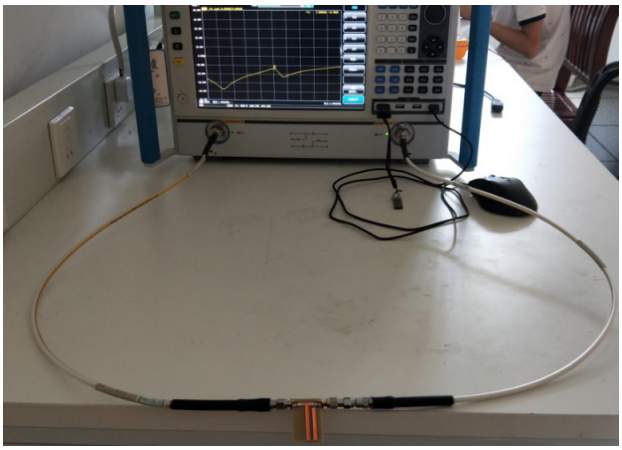

**FIGURE 8.** Configuration of Ti-NGD circuit prototype experimental setup.

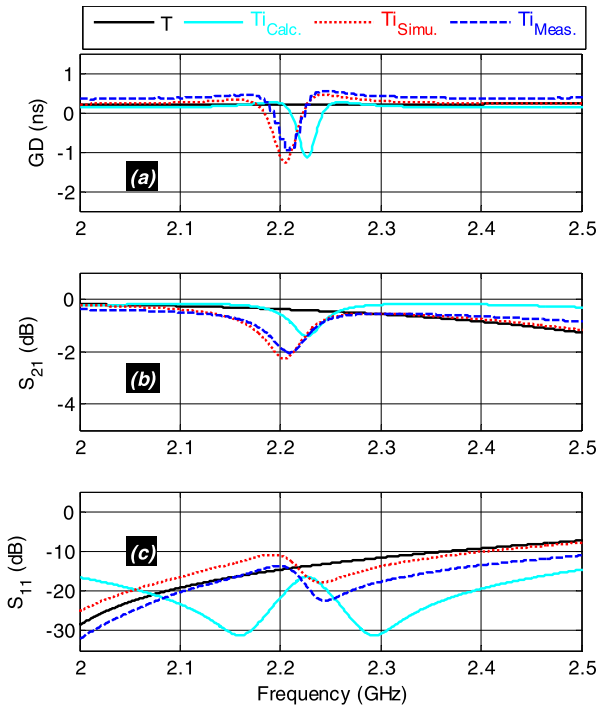


**FIGURE 9.** Comparisons of calculated, simulated and measured (a) GD and (b) transmission and reflection coefficients from the Ti prototype shown in Figs. 4.

proposed Ti topology is susceptible to behave as a bandpass NGD function.

As plotted in Fig. 9(a), the Ti topology circuit indicates optimal NGD values of about −1.2 ns −1.27 ns and −1 ns from calculation (“Calc.”), simulation (“Simu.”) and measurement (“Meas.”), respectively. The measured center frequency is about 2.21 GHz. Moreover, the transmission coefficients shown in Fig. 9(b) is widely better than −2.5 dB. Additionally, as depicted in Fig. 9(c), the reflection coefficients are better than −13 dB in the NGD bandwidth. The differences between the calculated, simulated and experimental results of $S_{11}$ are notably due to the numerical computation inaccuracies, the substrate dispersion loss, the metallization

**TABLE 5. Calculated, simulated and experimented NGD performances.**

| *Validation method* | $f_0$ (GHz) | $GD_0$ (ns) | $BW$ (MHz) | $S_{21}(f_0)$ (dB) | $S_{11}(f_0)$ (dB) |
|---|---|---|---|---|---|
| Calculation | 2.247 | -1.1 | 35 | -1.65 | -15.0 |
| Simulation | 2.206 | -1.20 | 34 | -2.26 | -11.5 |
| Measurement | 2.21 | -1 | 32 | -2.1 | -13.6 |

**TABLE 6. Comparison between the investigated Ti and other NGD circuit performances.**

| Ref. | $f_0$ (GHz) | GD($f_0$) (ns) | $S_{21}(f_0)$ (dB) | $S_{11}(f_0)$ (dB) | FoM | Use of lossy resistor |
|---|---|---|---|---|---|---|
| [28] | 1.34 | -1.3 | -3.16 | -10.33 | 0.0506 | Yes |
| [29] | 2.15 | -1.8 | -5.5 | * | 0.0401 | Yes |
| [30] | 1 | 1.5 | -33 | -25 | 0.0133 | Yes |
| [31] | 1.89 | -1 | -1.7 | -15 | 0.0164 | No |
| This work | 2.21 | -1 | -2.1 | -13 | 0.0314 | No |

(*) No data in the origin references, simulation results indicate it is not better than -10 dB.

skin effect, and the fabricated circuit imperfection in the considered working frequency.

#### 3) DISCUSSION ON Ti NGD MODELLING

Compared to the crosstalk modelling available in the literature [1]–[14], the proposed one enables:

- To understand with analytical expression an unfamiliar phenomenon as NGD with consideration of particular shape TL including both coupling coefficient and delay parameters,
- The simplicity of the developed analytical modelling method,
- And the developed method presents computation speed less than tens milliseconds by using a PC equipped a single-core processor Intel® Core™ i7-4790 CPU @ 3.60 GHz and 32 GB physical RAM with 64-bits Windows 7.

### D. DISCUSSION ON STATE-OF-THE-ART NGD PERFORMANCES

In addition to the established theory and validation results, it would be necessary to situate the achievement of the presented Ti shape microstrip topology compared to the published NGD circuits in the literature. Acting as passive microwave circuit, the NGD circuit performance depends on the NGD level $\tau$, NGD bandwidth $\Delta\omega$, transmission coefficient $S_{21}$ and reflection coefficient $S_{11}$. The NGD figure-of-merit (FoM) is defined by:

$$FoM = GD(\omega_0) \cdot \Delta\omega \cdot \sqrt{\frac{S_{21}(\omega_0)}{S_{11}(\omega_0)}}. \tag{46}$$

Table 6 introduces the comparison of the tested Ti NGD circuit and the other literature [28]–[31]. Compared to the NGD circuits designed in [28]–[30], the Ti circuit shows advantage in design simplicity and fully distributed circuit without using any lossy element component. Compared to [30], [31], the Ti-shape circuit shows better FoM.

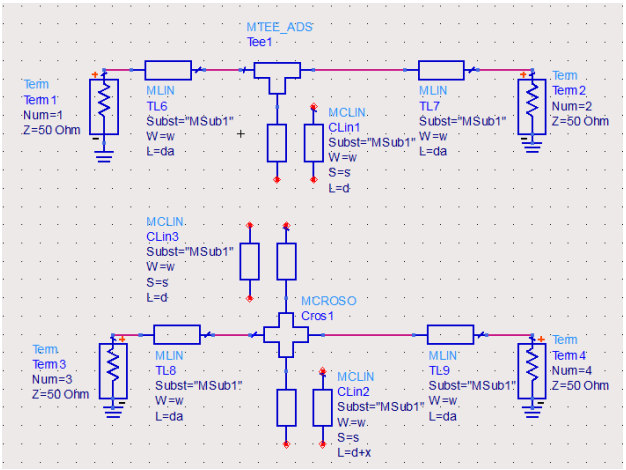


**FIGURE 10. ADS® design of one- and two-cell Ti POCs.**

## V. DUAL-BAND AND WIDENED BAND Ti NGD CIRCUIT SIMULATIONS

One of the main benefits of Ti NGD topology concerns the design simplicity. This design simplicity enables to implement several cells-based circuits. Such a design enables to improve the NGD bandwidth or also multi-band operation. The present section is focused on the design feasibility of two-cells based circuit to widen the NGD bandwidth and also to propose an operation in two-disjointed frequency bands.

### A. DESCRIPTION OF TWO-CELLS Ti NGD DESIGN

Fig. 10 depicts the schematic design of one- and two-Ti cells based POC in the ADS® environment. These circuits are considered implemented on the same Cu-metallized FR4-substrate specified in Table 1. The one cell circuit is implemented with same width, $w$, lengths ($d_a$, $d$) and interspace s as the circuit proposed in Figs. 4. However, the two-cell circuit is built with:

- One cell Ti-circuit with physical sizes ($w$, $d_a$, $d$),
- And the two cells based Ti-circuit with physical sizes ($w$, $d_a$, $d_0 + x$). The generation of dual-band or widened band aspect depends essentially on the extra-length, $x$.

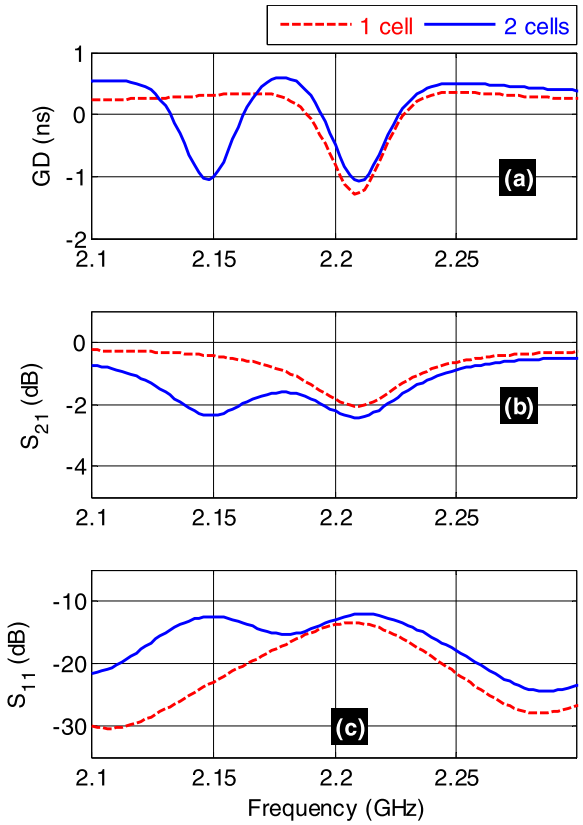


**FIGURE 11.** Comparisons of simulated 1- and 2-cell Ti NGD circuits: (a) GD, (b) transmission and (c) reflection coefficients.

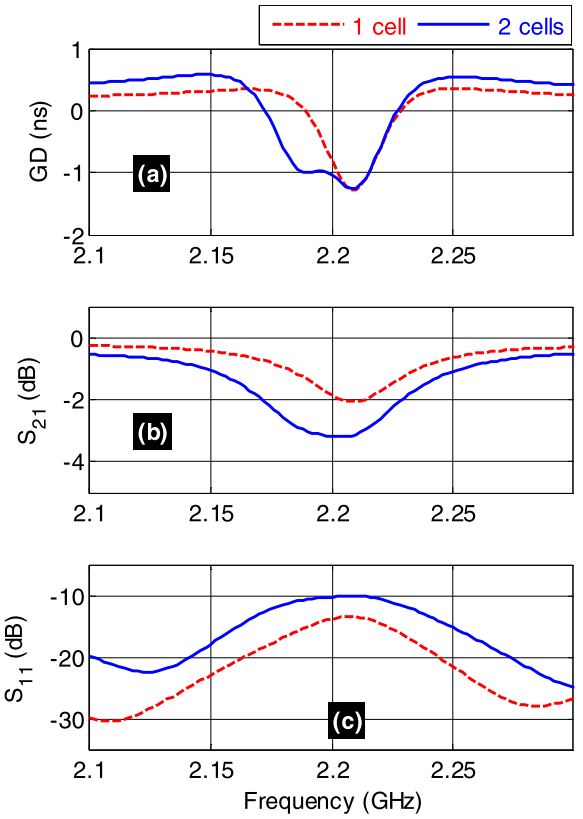


**FIGURE 12.** Comparisons of simulated one- and two-cell Ti NGD circuits: (a) GD, (b) transmission and (c) reflection coefficients.

### B. DUAL-BAND NGD RESULTS WITH TWO-CELLS Ti BASED CIRCUIT

Figs. 11 display the comparison between the ADS® simulated results from one- (plotted in dashed red curve) and double- (plotted in solid blue curve) cells based Ti-circuit. In this case, the overlength, $x$, was fixed to 1 mm.

As illustrated in Fig. 11(a), the GD response presents two bandwidths centered at $f_1 = 2.21$ GHz and $f_2 = 2.148$ GHz. It is clear that the NGD with center frequency, $f_1$, corresponds to the CL length, $d$. Then, the other NGD band represents the influence of CL length, $d + x$. However, the slight difference between the NGD value of about 0.2 ns is observed. The transmission coefficient, $S_{21}$, is close to $-2$ dB around the two different center frequencies as depicted in Fig. 11(b). Furthermore, the flatness of the transmission coefficient in the NGD bandwidth is less than 1 dB. Finally, the dual-band Ti NGD response guarantee a very good access matching better than $-10$ dB as seen in Fig. 11(c).

### C. WIDENED BAND NGD RESULTS WITH TWO-CELLS Ti BASED CIRCUIT

By taking $x = 0.36$ mm, we obtain the simulated results of two-Ti cell circuit given in Figs. 12. The two-cell results are plotted in blue solid line. As explained by Fig. 12(a), the NGD bandwidth is considerably increased to about $\Delta f \approx 56$ MHz. Compared to one cell, the increase of the bandwidth is more than 30%. However, as displayed in Fig. 12(b), $S_{21}$ is slightly dropped to about $-3.2$ dB around the NGD center frequency. The flatness of $S_{21}$ remains lower than 1 dB in the NGD bandwidth.

The reflection coefficient is of about $-10$ dB around the NGD center frequency as can be seen in Fig. 12(c).

## VI. CONCLUSION

An innovative analytical modelling of interconnect line topology constituted by particular shape of named Ti topology NGD is investigated.

The S-matrix modelling theory is not only innovative in term of the topology identification but also on the analysis method of CL structure by taking into account the CL attenuation and propagation delay. Based on the S-matrix analysis, the analytical equivalent model of reflection and transmission parameters is established. Then, phenomenological analysis based on the GD is established in function of the Ti topology parameters.

Experimental validation was discussed with a circuit prototype implemented in microstrip technology. An excellent agreement between simulations and measurements was observed. The measured GD value of $-1$ ns and transmission coefficient better than $-2.1$ dB were occurred at the center frequency of approximately 2.2 GHz.

## REFERENCES


[1] S. Roy and A. Dounavis, "Efficient delay and crosstalk modeling of RLC interconnects using delay algebraic equations," *IEEE Trans. Very Large Scale Integr. (VLSI) Syst.*, vol. 19, no. 2, pp. 342–346, Feb. 2011.

[2] M. Choi, J.-Y. Sim, H.-J. Park, and B. Kim, "An approximate closed-form transfer function model for diverse differential interconnects," *IEEE Trans. Circuits Syst. I, Reg. Papers*, vol. 62, no. 5, pp. 1335–1344, May 2015.

[3] S. Sun, G. Liu, J. L. Drewniak, and D. J. Pommerenke, "Hand-assembled cable bundle modeling for crosstalk and common-mode radiation prediction," *IEEE Trans. Electromagn. Compat.*, vol. 49, no. 3, pp. 708–718, Aug. 2007.

[4] A. Shoory, M. Rubinstein, A. Rubinstein, C. Romero, N. Mora, and F. Rachidi, "Application of the cascaded transmission line theory of paul and McKnight to the evaluation of NEXT and FEXT in twisted wire pair bundles," *IEEE Trans. Electromagn. Compat.*, vol. 55, no. 4, pp. 648–656, Aug. 2013.

[5] C. R. Paul, "Derivation of common impedance coupling from the transmission-line equations," *IEEE Trans. Electromagn. Compat.*, vol. 34, no. 3, pp. 315–319, Aug. 1992.

[6] S. Shiran, B. Reiser, and H. Cory, "A probabilistic method for the evaluation of coupling between transmission lines," *IEEE Trans. Electromagn. Compat.*, vol. 35, no. 3, pp. 387–393, Aug. 1993.

[7] D. Brooks, *Crosstalk Coupling: Single-Ended Vs. Differential*. Lane Issaquah, WA, USA: Tech. Publication, President UltraCAD Design, Sep. 2005, pp. 1–19. [Online]. Available: https://www.ultracad.com/mentor/crosstalk_coupling.pdf

[8] T. Zeeff, M. Xu, and C. Olsen, "Coupling between a microstrip trace pair," PDF, Kansas City, MO, USA, White Paper tc9, 2003, pp. 1–4. [Online]. Available: http://www.ewh.ieee.org/cmte/tc9/summary/co_mic/web03.pdf

[9] W. Shi and J. Fang, "Evaluation of closed-form crosstalk models of coupled transmission lines," *IEEE Trans. Adv. Packag.*, vol. 22, no. 2, pp. 174–181, May 1999.

[10] D. Bellan, S. A. Pignari, and G. Spadacini, "Characterisation of crosstalk in terms of mean value and standard deviation," *IEE Proc. Sci., Meas. Technol.*, vol. 150, no. 6, pp. 289–295, Nov. 2003.

[11] M. Wu, D. G. Beetner, T. H. Hubing, H. Ke, and S. Sun, "Statistical prediction of 'reasonable worst-case' crosstalk in cable bundles," *IEEE Trans. Electromagn. Compat.*, vol. 51, no. 3, pp. 842–851, Aug. 2009.

[12] C. Jullien, P. Besnier, M. Dunand, and I. Junqua, "Advanced modeling of crosstalk between an unshielded twisted pair cable and an unshielded wire above a ground plane," *IEEE Trans. Electromagn. Compat.*, vol. 55, no. 1, pp. 183–194, Feb. 2013.

[13] M. S. Halligan and D. G. Beetner, "Maximum crosstalk estimation in lossless and homogeneous transmission lines," *IEEE Trans. Microw. Theory Techn.*, vol. 62, no. 9, pp. 1953–1961, Sep. 2014.

[14] T. Ciamulski and W. K. Gwarek, "On eliminating crosstalk within multiconductor transmission lines," *IEEE Microw. Wireless Compon. Lett.*, vol. 14, no. 6, pp. 298–300, Jun. 2004.

[15] B. Ravelo, "Theory of coupled line coupler-based negative group delay microwave circuit," *IEEE Trans. Microw. Theory Techn.*, vol. 64, no. 11, pp. 3604–3611, Nov. 2016.

[16] R. Das, Q. Zhang, and H. Liu, "Lossy coupling matrix synthesis approach for the realization of negative group delay response," *IEEE Access*, vol. 6, pp. 1916–1926, 2018.

[17] F. Wan, N. Li, B. Ravelo, Q. Ji, and J. Ge, "S-parameter model of three parallel interconnect lines generating negative group-delay effect," *IEEE Access*, vol. 6, pp. 57152–57159, 2018.

[18] S. Lucyszyn and I. D. Robertson, "Analog reflection topology building blocks for adaptive microwave signal processing applications," *IEEE Trans. Microw. Theory Techn.*, vol. 43, no. 3, pp. 601–611, Mar. 1995.

[19] C. D. Broomfield and J. K. A. Everard, "Broadband negative group delay networks for compensation of oscillators and filters," *Electron. Papers*, vol. 36, no. 23, pp. 1931–1933, Nov. 2000.

[20] G. Chaudhary and Y. Jeong, "Negative group delay phenomenon analysis using finite unloaded quality factor resonators," *Prog. Electromagn. Res.*, vol. 156, pp. 55–62, 2016.

[21] Z. A. Khan, "A novel transmission line structure for high-speed high-density copper interconnects," *IEEE Trans. Compon., Packag., Manuf. Technol.*, vol. 6, no. 7, pp. 1077–1086, Jul. 2016.

[22] D. V. Ginste, D. D. Zutter, D. Deschrijver, T. Dhaene, P. Manfredi, and F. Canavero, "Stochastic modeling-based variability analysis of on-chip interconnects," *IEEE Trans. Compon., Packag., Manuf. Technol.*, vol. 3, no. 7, pp. 1244–1251, Jul. 2012.

[23] B. Ravelo, "Delay modelling of high-speed distributed interconnect for the signal integrity prediction," *Eur. Phys. J. Appl. Phys. (EPJAP)*, vol. 57, pp. 1–8, Feb. 2012.

[24] T. Shao, Z. Wang, S. Fang, H. Liu, and S. Fu, "A compact transmission-line self-matched negative group delay microwave circuit," *IEEE Access*, vol. 5, pp. 22836–22843, 2017.

[25] Z. Wang, Y. Cao, T. Shao, S. Fang, and Y. Liu, "A negative group delay microwave circuit based on signal interference techniques," *IEEE Microw. Wireless Compon. Lett.*, vol. 28, no. 4, pp. 290–292, Apr. 2018.

[26] B. Ravelo, "Tee power divider and combiner based negative group delay topology," *Int. J. RF Microw. Comput.-Aided Eng.*, vol. 28, no. 9, pp. 1–9, Nov. 2018.

[27] G. Chaudhary and Y. Jeong, "Low signal-attenuation negative group-delay network topologies using coupled lines," *IEEE Trans. Microw. Theory Techn.*, vol. 62, no. 10, pp. 2316–2324, Oct. 2014.

[28] F. Wan, L. Wu, B. Ravelo, and J. Ge, "Analysis of interconnect line coupled with a radial-stub terminated negative group delay circuit," *IEEE Trans. Electromagn. Compat.*, early access, Aug. 30, 2019, doi: 10.1109/TEMC.2019.2936266.

[29] G. Chaudhary, P. Kim, J. Kim, Y. Jeong, and J. Lim, "Coupled line negative group delay circuits with very low signal attenuation and multiple-poles characteristics," in *Proc. 44th Eur. Microw. Conf.*, Oct. 2014, pp. 25–28.

[30] C.-T.-M. Wu and T. Itoh, "Maximally flat negative group-delay circuit: A microwave transversal filter approach," *IEEE Trans. Microw. Theory Techn.*, vol. 62, no. 6, pp. 1330–1342, Jun. 2014.

[31] F. Wan, N. Li, B. Ravelo, W. Rahajandraibe, and S. Lalléchère, "Design of =|= shape stub based negative group delay circuit," *IEEE Design & Test*, early access, Jun. 12, 2020, doi: 10.1109/MDAT.2020.3002149.